

Asymptotic radiative transfer

A C Selden*

ABSTRACT

Asymptotic radiative transfer (ART), like diffusion theory, assumes the angular intensity distribution incident at a boundary is identical with that in the depth of the scattering medium. However, the asymptotic intensity profile and accurate attenuation coefficient corresponding to the scattering phase function are used in preference to the P1 approximations of diffusion theory, thereby extending the range of asymptotic radiative transfer to the lowest particle scattering albedoes. Asymptotic calculations for scattering media with refracting boundaries are compared with diffusion theory and accurate radiative transfer data to illustrate this. The error involved can be further reduced by the addition of a suitable boundary transient.

**adrian_selden@yahoo.com*

Asymptotic theory

Introduction

The asymptotic approach employs the partial fluxes J_+ , J_- obtained by integrating the angular intensity $I(\mu)$ over the forward and backward hemispheres [1, 2], where μ is the direction cosine with respect to the symmetry axis. In contrast to diffusion analysis, which assumes a mild cosine intensity variation and approximate diffuse attenuation coefficient [3], the asymptotic intensity distribution $I_{as}(\mu)$ valid in the depth of the scattering medium and exact attenuation coefficient (least eigenvalue λ_0) corresponding to the scattering phase function $p(\mu)$ are used here [4]. The asymptotic calculations yield more accurate results than diffusion theory, they minimize the number of boundary equations compared with other methods, thereby reducing the numerical effort in multilayer calculations, and are applicable over a broad range of scattering albedo $\varpi \in [0, 1]$.

Partial fluxes

The partial fluxes J_+ , J_- are defined as [1, 2]

$$J_+ = \frac{1}{2} \int_0^1 I(\mu) \mu d\mu \quad (1a)$$

$$J_- = \frac{1}{2} \int_0^1 I(-\mu) \mu d\mu \quad (1b)$$

Here $I(\mu)$ corresponds to the asymptotic angular intensity distribution $I_{as}(\mu) \Rightarrow g(\mu, \lambda)$, the solution of the characteristic equation of radiative transfer valid in the depth of the scattering medium [Appendix A]. The asymptotic method proceeds by formulating the boundary equations in terms of the partial fluxes, yielding integrated boundary equations (IBEs) for the problem posed.

Integrated boundary equations

At a specularly reflecting boundary, the forward intensity $I(\mu > 0)$ equates to the reflected (backward) intensity $I(\mu < 0)$ viz.

$$I(\mu) = R(\mu) I(-\mu) \quad (2a)$$

and for a diffusely reflecting boundary

$$I(\mu) = R(\mu) J_- \quad (2b)$$

where $R(\mu)$ is the boundary reflectance, which in general is a function of μ . At a refracting boundary, $R(\mu)$ is given by the Fresnel reflectance function for unpolarised light [1]

$$R(\mu) = \frac{1}{2} \left[\left(\frac{\mu - n\mu_0}{\mu + n\mu_0} \right)^2 + \left(\frac{\mu_0 - n\mu}{\mu_0 + n\mu} \right)^2 \right] \quad \mu \geq \mu_c \quad (3)$$

and $R(\mu) \equiv 1$ for $\mu \leq \mu_c$, the cosine of the critical angle: $\mu_c^2 = 1-1/n^2$ for refractive index n . Clearly, the reflected intensity profile $I(\mu>0)$ has a ‘hole’ for $\mu \in |\mu_c, 1|$, corresponding to low reflectance within the cone defined by the critical angle (Fig 1). Multiplying eqns (2a, 2b) by $\mu d\mu$ and integrating, we obtain the integrated boundary equations (IBEs) for specular and diffuse reflection respectively

$$\begin{aligned} J_+ &= \frac{1}{2} \int_0^1 I(\mu) \mu d\mu = \frac{1}{2} \int_0^1 R(\mu) I(-\mu) \mu d\mu \\ J_+ &= \frac{1}{2} \int_0^1 I(\mu) \mu d\mu = J_- \int_0^1 R(\mu) \mu d\mu \end{aligned} \quad (4a,b)$$

Illuminated half space

At the boundary of a refracting medium illuminated by a surface source $S(\mu_0)$, the internal forward intensity $I(\mu)$ equates to the specularly reflected backward intensity $R(\mu)I(-\mu)$ plus the transmitted source intensity concentrated by a factor n^2

$$I(\mu) = R(\mu)I(-\mu) + n^2 [1 - R(\mu_0)] S(\mu_0) \quad (5)$$

where the interior and exterior cosines μ , μ_0 are related via Snell’s law viz.[1]

$$1 - \mu_0^2 = n^2 (1 - \mu^2)$$

whence

$$\mu_0 d\mu_0 = n^2 \mu d\mu \quad (6 a,b)$$

Thus the integrated boundary equation (IBE) for the asymptotic intensity $I_{as}(\mu) \Rightarrow A_0 g(\mu, \lambda)$ is

$$A_0 \int_0^1 [g(\mu, \lambda) - R(\mu)g(-\mu, \lambda)] \mu d\mu = \int_0^1 [1 - R(\mu_0)] S(\mu_0) \mu_0 d\mu_0 \quad (7)$$

enabling the coefficient A_0 and half-space albedo A^* to be determined viz.

$$A^* = A_0 \int_{\mu_c}^1 [1 - R(\mu)] g(-\mu, \lambda) \mu d\mu \quad (8)$$

which can be written symbolically as

$$A^* = \frac{S(n)F(n, \lambda)}{C(n, \lambda)} \quad (9)$$

with $S(n)$, $F(n, \lambda)$, $C(n, \lambda)$ defined in eqns (12), (14) below

Dielectric slab

For a dielectric slab of width $d = 2a$, the asymptotic intensity may be written as

$$I(x, \mu) = A e^{-\lambda x} g(\mu, \lambda) + B e^{\lambda x} g(-\mu, \lambda) \quad x \in (-a, a) \quad (10)$$

representing the intensity as the sum of the forward ($\mu>0$) and backward ($\mu<0$) asymptotic angular intensities $g(\mu, \lambda)$, $g(-\mu, \lambda)$ with coefficients A and B , where λ is the attenuation coefficient. Applying boundary equations (2) and (5), multiplying by $\mu d\mu$ and integrating

over $\mu \in |0,1|$ we obtain two IBEs (for $x = a, -a$)

$$\begin{aligned} Ae^{\lambda a}C(n, \lambda) + Be^{-\lambda a}D(n, \lambda) &= S(n) \\ Ae^{-\lambda a}D(n, \lambda) + Be^{\lambda a}C(n, \lambda) &= 0 \end{aligned} \quad (11a,b)$$

which determine the unknown coefficients A, B in terms of source strength S_0 and attenuation parameter λa , where

$$\begin{aligned} C(n, \lambda) &= \int_0^1 [g(\mu, \lambda) - R(\mu)g(-\mu, \lambda)]\mu d\mu \\ D(n, \lambda) &= \int_0^1 [g(-\mu, \lambda) - R(\mu)g(\mu, \lambda)]\mu d\mu \\ S(n) &= \int_0^1 [1 - R(\mu_0)]S(\mu_0)\mu_0 d\mu_0 \end{aligned} \quad (12a,b,c)$$

whence the slab albedo A^* and diffuse transmittance T^* are given by

$$\begin{aligned} A^* &= \frac{S(n)[C(n, \lambda)F(n, \lambda) - D(n, \lambda)E(n, \lambda)\exp(-4\lambda a)]}{C^2(n, \lambda) - D^2(n, \lambda)\exp(-4\lambda a)} \\ T^* &= \frac{S(n)\exp(-2\lambda a)[C(n, \lambda)E(n, \lambda) - D(n, \lambda)F(n, \lambda)]}{C^2(n, \lambda) - D^2(n, \lambda)\exp(-4\lambda a)} \end{aligned} \quad (13a,b)$$

where

$$\begin{aligned} E(n, \lambda) &= \int_{\mu_c}^1 [1 - R(\mu)]g(\mu, \lambda)\mu d\mu \\ F(n, \lambda) &= \int_{\mu_c}^1 [1 - R(\mu)]g(-\mu, \lambda)\mu d\mu \end{aligned} \quad (14a,b)$$

Interface

At an interface between two dielectric scattering media with refractive index ratio $n = n_1/n_2$, the intensity leaving the interface equates to the reflected incident intensity plus the intensity transmitted (and refracted) by the adjoining medium viz.

$$\begin{aligned} I(\mu) &= R(\mu)I(-\mu) + n^2[1 - R(\mu')]I(\mu') \\ I(-\mu') &= R(\mu')I(\mu') + [1 - R(\mu)]I(-\mu) / n^2 \end{aligned} \quad (15a,b)$$

where μ, μ' are the cosines in the adjoining media, related as in eq (6a).

The IBEs are formed as above, with $I(x, \mu), I(x', \mu')$ expressed as in eqn (10), with coefficients A_1, B_1, A_2, B_2 . The IBEs are expressed in matrix form as

$$\begin{bmatrix} D(n_1, \lambda_1) & C(n_1, \lambda_1) \\ E(n_1, \lambda_1) & F(n_1, \lambda_1) \end{bmatrix} \begin{bmatrix} A_1 \\ B_1 \end{bmatrix} = \begin{bmatrix} F(n_2, \lambda_2) & E(n_2, \lambda_2) \\ C(n_2, \lambda_2) & D(n_2, \lambda_2) \end{bmatrix} \begin{bmatrix} A_2 \\ B_2 \end{bmatrix} \quad (16)$$

with $C(n, \lambda), D(n, \lambda), E(n, \lambda), F(n, \lambda)$ defined as above (eqns (12a,b,c), (14a,b)).

A sample calculation of the flux discontinuity at an interface between two half-spaces with uniform sources is given in Appendix B. Asymptotic and diffusion results are compared with radiative transfer (RT) in Fig 2. Tables of $C(n, \lambda), D(n, \lambda), E(n, \lambda), F(n, \lambda)$ vs ϖ , with analytic solutions of eqns (15a,b) and their diffusion counterparts, are presented in Appendix C.

Double layer

The IBEs for a double layer, consisting of two free boundaries plus an interface, are formulated by combining boundary eqns (11a,b) and (15a,b), yielding four IBEs for the four intensity coefficients A_1, B_1, A_2, B_2 , written in matrix form as $\mathbf{M}=\mathbf{A}\mathbf{S}$, where

$$\mathbf{M} = \begin{bmatrix} C(n_1, \lambda_1)e^{\lambda_1 a_1} & D(n_1, \lambda_1)e^{-\lambda_1 a_1} & 0 & 0 \\ 0 & 0 & D(n_2, \lambda_2)e^{\lambda_2 a_2} & C(n_2, \lambda_2)e^{-\lambda_2 a_2} \\ D(n_{12}, \lambda_1)e^{\lambda_1 a_1} & C(n_{12}, \lambda_1)e^{-\lambda_1 a_1} & -F(n_{21}, \lambda_2)e^{\lambda_2 a_2} & -E(n_{21}, \lambda_2)e^{-\lambda_2 a_2} \\ E(n_{12}, \lambda_1)e^{\lambda_1 a_1} & F(n_{12}, \lambda_1)e^{-\lambda_1 a_1} & -C(n_{21}, \lambda_2)e^{\lambda_2 a_2} & -D(n_{21}, \lambda_2)e^{-\lambda_2 a_2} \end{bmatrix} \quad \mathbf{A} = \begin{bmatrix} A_1 \\ B_1 \\ A_2 \\ B_2 \end{bmatrix} \quad \mathbf{S} = \begin{bmatrix} S_0 \\ 0 \\ 0 \\ 0 \end{bmatrix} \quad (17)$$

Multilayers

The interface eqns (15a,b) can be extended to multilayer media, the IBEs at each interface relating the intensity coefficients A_k, B_k for each layer to those of the adjacent layer. These are solved sequentially via matrix inversion (Appendix C) to fit external boundary conditions e.g. surface sources or free boundaries. Thus for each pair of adjacent layers ($k, k+1$)

$$\mathbf{M}_k \mathbf{A}'_k = \mathbf{M}_{k+1} \mathbf{A}''_{k+1} \quad (18a)$$

where

$$\mathbf{A}'_k = \begin{bmatrix} A_k e^{-\lambda_k a_k} \\ B_k e^{\lambda_k a_k} \end{bmatrix} \quad (18b)$$

$$\mathbf{A}''_{k+1} = \begin{bmatrix} A_{k+1} e^{\lambda_{k+1} a_{k+1}} \\ B_{k+1} e^{-\lambda_{k+1} a_{k+1}} \end{bmatrix}$$

and

$$\mathbf{M}_k = \begin{bmatrix} D(n_{k,k+1}, \lambda_k) & C(n_{k,k+1}, \lambda_k) \\ E(n_{k,k+1}, \lambda_k) & F(n_{k,k+1}, \lambda_k) \end{bmatrix} \quad (18c)$$

$$\mathbf{M}_{k+1} = \begin{bmatrix} F(n_{k+1,k}, \lambda_{k+1}) & E(n_{k+1,k}, \lambda_{k+1}) \\ C(n_{k+1,k}, \lambda_{k+1}) & D(n_{k+1,k}, \lambda_{k+1}) \end{bmatrix}$$

Boundary transient

The accuracy of asymptotic theory can be enhanced by the addition of a boundary transient, as in the K-integral method [5]. Thus, expressing the boundary intensity $I(0, \mu)$ as the sum of the asymptotic intensity $I_{as}(0, \mu) \Rightarrow g(\mu, \lambda)$ and a boundary transient $\psi(\mu)$

$$I(0, \mu) = g(\mu, \lambda) + \psi(\mu) \quad (19)$$

the relative magnitudes of $\psi(\mu)$ and $g(\mu, \lambda)$ being determined by taking two moments of the boundary equations with weight functions $g_i(\mu)$ ($i=1,2$) [5]. Further analysis and results for a half-space are presented in the Supplement.

Diffusion theory

Diffusion theory employs the scalar flux (flux density) φ and vector flux $J = -D\nabla\varphi$ (where D is the diffusion coefficient), defined as follows [6]

$$\begin{aligned}\varphi &= \frac{1}{2} \int_{-1}^1 I(\mu) d\mu \\ J &= \frac{1}{2} \int_{-1}^1 I(\mu) \mu d\mu\end{aligned}\quad (20)$$

Expanding the angular dependence of φ at the boundary to first order in μ

$$\begin{aligned}\varphi(0, \mu) &= \frac{1}{2} \varphi_0(0) + \frac{3}{2} \mu \varphi_1(0) \\ \varphi_1(0) &= -D\varphi_0'(0)\end{aligned}\quad (21)$$

applying boundary eq (2a), multiplying by μ and integrating, we find [7]

$$\varphi_0(0) = \lambda_s \varphi_0'(0) \quad (22)$$

$$\lambda_s = \frac{2 [1 + 3R_2]}{3 [1 - 2R_1]} \quad (23)$$

Here λ_s is the linear extrapolation distance beyond the boundary, where $\varphi_0(x) \Rightarrow 0$, and R_1, R_2 are defined by

$$R_n = \int_0^1 R(\mu) \mu^n d\mu \quad (24)$$

Similarly, RT analysis yields a linear extrapolation distance $d = d(n, \kappa)$, dependent on n and extinction coefficient κ [1, 7]. Inserting eq (21) in boundary eq (5) and integrating, we obtain an analytic expression for the albedo of a half-space with refracting boundary [8]

$$A^* = \bar{q}_s \frac{1 - 2R_1 - 2D\kappa(1 - 3R_2)}{1 - 2R_1 + 2D\kappa(1 + 3R_2)} \quad (25)$$

with source term

$$\bar{q}_s = \int_0^1 q(\mu) [1 - R(\mu)] \mu d\mu \quad (26)$$

and [9, 10]

$$D\kappa = (1 - \varpi) / \kappa \quad (27)$$

where κ is the extinction coefficient and D the diffusion coefficient. For a non-refracting boundary ($n=1$) $R_1, R_2 \equiv 0$ and eqn (25) reduces to

$$A^* = \bar{q}_s \frac{1 - 2D\kappa}{1 + 2D\kappa} \quad (28)$$

The diffusion analysis is readily extended to a finite layer i.e. slab geometry viz.

$$\varphi(x) = Ae^{-\kappa x} + Be^{\kappa x} \quad x \in [-a, a] \quad (29)$$

where $2a$ is the slab width. Applying boundary equations (2), (5) we find

$$\begin{aligned} (1-2R_1)(Ae^{\kappa a} + Be^{-\kappa a}) + 2D\kappa(1+3R_2)(Ae^{\kappa a} - Be^{-\kappa a}) &= 4\bar{q}_s \\ (1-2R_1)(Ae^{-\kappa a} + Be^{\kappa a}) + 2D\kappa(1+3R_2)(Ae^{-\kappa a} - Be^{\kappa a}) &= 0 \end{aligned} \quad (30a,b)$$

Solving for A, B yields the boundary fluxes $\varphi(a)$, $\varphi(-a)$ for determining the slab albedo A^* and diffuse transmittance T^* viz.

$$\begin{aligned} A^* &= q_s \frac{[\beta_1 - (\alpha_2 / \alpha_1)\beta_2 \exp(-4\kappa a)]}{\alpha_1[1 - (\alpha_2 / \alpha_1)^2 \exp(-4\kappa a)]} \\ T^* &= q_s \frac{[\beta_2 - (\alpha_2 / \alpha_1)\beta_1] \exp(-2\kappa a)}{\alpha_1[1 - (\alpha_2 / \alpha_1)^2 \exp(-4\kappa a)]} \end{aligned} \quad (31a,b)$$

where

$$\begin{aligned} \alpha_1 &= 1 - 2R_1 + 2D\kappa[1 + 3R_2] \\ \alpha_2 &= 1 - 2R_1 - 2D\kappa[1 + 3R_2] \\ \beta_1 &= 1 - 2R_1 - 2D\kappa[1 - 3R_2] \\ \beta_2 &= 1 - 2R_1 + 2D\kappa[1 - 3R_2] \end{aligned} \quad (32a,b,c,d)$$

The diffusion boundary equations at an interface between two refractive scattering media are

$$\begin{aligned} \varphi_2 &= n^2 \varphi_1 + C_0(n_{21})J_{1,2} \\ J_{1,2} &= J_1 = J_2 \end{aligned} \quad (33a,b)$$

where $C_0(n_{21})$ is a monotonic function of refractive index ratio $n_{21} = n_2/n_1$ [1, 5]. Dividing by φ_1 we find

$$\varphi_2 / \varphi_1 = n^2 + C_0(n_{21}) < \mu_1 > \quad (34)$$

where $< \mu_1 > = J_1 / \varphi_1$ is the mean cosine of the radiance at the boundary [11]. Inserting $\varphi(0)$ from eqn (29) in eqns (33a,b) yields

$$\begin{aligned} A_2 + B_2 &= A_1(n_{21}^2 + C_0(n_{21})D_1\lambda_1) + B_1(n_{21}^2 - C_0(n_{21})D_1\lambda_1) \\ D_1\lambda_1[A_1 - B_1] &= D_2\lambda_2[A_2 - B_2] \end{aligned} \quad (35a,b)$$

allowing A_2 , B_2 to be expressed in terms of A_1 , B_1 as follows

$$\begin{aligned} A_2 &= \frac{1}{2}[n_{21}^2 + C_0(n_{21})D_1\lambda_1 + \frac{D_1\lambda_1}{D_2\lambda_2}]A_1 \\ &\quad + \frac{1}{2}[n_{21}^2 - C_0(n_{21})D_1\lambda_1 - \frac{D_1\lambda_1}{D_2\lambda_2}]B_1 \end{aligned} \quad (36a)$$

$$\begin{aligned} B_2 &= \frac{1}{2}[n_{21}^2 + C_0(n_{21})D_1\lambda_1 - \frac{D_1\lambda_1}{D_2\lambda_2}]A_1 \\ &\quad + \frac{1}{2}[n_{21}^2 - C_0(n_{21})D_1\lambda_1 + \frac{D_1\lambda_1}{D_2\lambda_2}]B_1 \end{aligned} \quad (36b)$$

Interface boundary equations are required for multi-layer analysis, in addition to those for the external surfaces, yielding e.g. a 4x4 matrix for the intensity coefficients of a double layer, analogous to eqn (16) for asymptotic RT theory. The multi-layer diffusion equations can be solved sequentially as above, expressing the coefficients A_{k+1} , B_{k+1} of the (k+1)th layer in terms of the coefficients A_k , B_k of the preceding kth layer [see Appendix C]

Results

The albedo A^* of a half-space illuminated by an obliquely incident uni-directional plane wave source is presented in Table I for scattering albedo $\varpi=0.99$, showing the dependence of A^* on the angle of incidence. The errors in the diffusion and asymptotic results are comparable (~2%-3%); a boundary correction reduces the error in the asymptotic result by more than an order of magnitude (~0.1%). The error in the diffusion result increases rapidly for lower scattering albedoes, reaching 100% for $\varpi=0.5$, while the asymptotic error remains below 10% (Figs 3 a-f). Results of calculations of the dependence of half-space albedo A^* on scattering albedo ϖ are shown in Tables II (a, b) for plane-wave and isotropic sources, the diffusion values increasing in error as ϖ diminishes, the asymptotic values remaining within a few percent of the RT data for the lowest scattering albedoes (<3% for $\varpi=0.3$). The asymptotic error is significantly less for isotropic illumination, remaining within $\pm 2\%$ for the full range of scattering albedo $\varpi \in [0, 1]$, whereas the error for plane-wave illumination has a maximum value of 8% when $\varpi=0.8$. The error is reduced by an order of magnitude with a suitable boundary correction (K-integral) (Fig 4 a,b). Similar results are found for a diffusing boundary (Fig 4 c,d). Results for the albedo A^* and diffuse transmittance T^* of a thick slab ($d=10$, $n=1.5$) with isotropic illumination [12] are presented in Table III. Note the precise agreement of the diffusion and asymptotic values for $\varpi \equiv 1$ (to 6 significant figures). For $\varpi < 1$, the diffusion error increases as ϖ diminishes, exceeding 100% for $\varpi < 0.5$, the asymptotic error having a maximum value <3% for $\varpi \sim 0.8-0.9$, decreasing thereafter (Fig 4e). Calculations with a boundary correction (K-integrals) achieve remarkable accuracy in this case, differing from the RT data by just 2 units in the 5th decimal [13]. The asymptotic flux density jump at an interface shows closer agreement with the K-integral calculations [5, 13] than diffusion (Table IV, Fig 2). Results for double-layers with differing refractive index are presented in Tables V, VI and Fig 4f for isotropic illumination, with similar results, the diffusion error exceeding 100% for $\varpi < 0.5$, the asymptotic error remaining below a maximum ~2% ($\varpi=0.8$). This is reduced by ~2 orders of magnitude with a suitable boundary correction, as above. However, plots of the internal intensity profiles incident at a refracting boundary

increasingly depart from the accurate RT profile, particularly for $\mu < \mu_c$ i.e. for total internal reflection (Supplement: Boundary flux). While this has little effect on the transmitted light (or the albedo), it does contribute to a significant error in the internal scalar flux (radiance) ϕ at the boundary, even with the K-integral correction. Again intensity profiles for isotropic illumination are much closer to the RT profile, resulting in more accurate results, as above.

Conclusions

From the examples given comparing the performance of asymptotic radiative transfer and diffusion theory, it is clear that the results converge for particle scattering albedo $\omega \Rightarrow 1$ as the angular intensities become increasingly isotropic, and that asymptotic RT is no more accurate than diffusion theory for scattering albedoes $\omega \geq 0.9$, errors of $\approx 3\% - 5\%$ occurring in calculations of half-space and slab albedo A^* for either. However, diffusion theory diverges increasingly rapidly for lower scattering albedoes, the error exceeding 100% for $\omega < 0.5$, while the error in asymptotic RT remains below 10% for plane-wave illumination, passing through a broad maximum for $\omega \approx 0.8$ and diminishing thereafter. Errors are lower for an isotropic source, the maximum albedo error $\Delta A^* \approx 3\%$ for $\omega \approx 0.8$, falling below 1% for $\omega < 0.5$. Since both diffusion and asymptotic RT satisfy the same small number of boundary conditions viz. one for an external surface, two for an interface, four for a double layer, the latter is clearly advantageous for approximate radiative transfer calculations of albedo and diffuse transmittance for media with lower particle scattering albedoes ($\omega \approx 0.8$ to $\omega \Rightarrow 0$). More accurate results can be achieved by the addition of a suitable boundary correction to the asymptotic angular intensity profile via the method of K-integrals [5].

Asymptotic analysis employs only low-order matrices with elements determined by the scattering albedo and refractive index, which can be calculated to high accuracy by gaussian quadrature and conveniently tabulated (Appendix C)

References

1. R. Aronson *Boundary conditions for diffusion of light* J Opt Soc Am A **12** (1995) 2532
2. S. Menon, Q. Su, R. Grobe *Velocity half-sphere model for multiple light scattering in turbid media* Phys. Rev. E **72** 041910 (2005)
3. S. A. Carp, S. A. Prahl, V. Venugopalan *Radiative transfer in the delta-P1 approximation: accuracy of fluence rate and optical penetration depth predictions in turbid semi-infinite media* J. Biomed. Opt. **9** 632-647 (2004)
4. V. I. Haltrin *One-parameter two-term Henyey-Greenstein phase function for light scattering in sea-water - Appendix A: Eigenvalues and radiance distribution of light in an asymptotic regime* Appl. Opt. **41** (2002) 1022-1028
5. M. M. R. Williams *An application of the K-integrals for solving the radiative transfer equation with Fresnel boundary conditions* J Quant Spectrosc Radiat Transf **107** (2007) 195-216
6. S. Chandrasekhar *Radiative Transfer* Dover (New York 1960)
7. M. M. R. Williams *The Milne problem with Fresnel reflection* J Phys A: Math. Gen. **38** (2005) 3841-3856
8. M. M. R. Williams *The albedo problem with Fresnel reflection* J Quant Spectrosc Radiat Transf **98** (2006) 358-378
9. R. Aronson, N. Corngold *Photon diffusion coefficient in an absorbing medium* J Opt Soc Am A **16** (1999) 1066-1071
10. D. C. Sahni, E. B. Dahl, N. G. Sjöstrand *Diffusion coefficient for photon transport in turbid media* Phys. Med. Biol. **48** (2003) 3969-3976
11. A. C. Selden *Analytic evaluation of diffuse fluence error in multilayer scattering media with discontinuous refractive index* J Biomed. Opt. **17** (2012) 035001
12. C-Y. Wu, B-T. Liou *Radiative transfer in a two-layer slab with Fresnel interfaces* J Quant Spectrosc Radiat Transf **56** (1996) 573-589
13. A. C. Selden *Accurate radiative transfer calculations for layered media* J Opt Soc Am A **33** (2016) 1409-1414
14. V. I. Haltrin *One-parameter two-term Henyey-Greenstein phase function for light scattering in seawater* Appl Opt **41** (2002) 1022-1028
15. H. C. van de Hulst *Light Scattering by Small Particles* Dover Publications (1981)

Appendix A

The asymptotic angular intensity distribution $g(\mu, \lambda)$ is the solution of the characteristic equation of radiative transfer valid in the depth of the scattering medium [5]

$$(1 - \lambda\mu)g(\mu, \lambda) = \varpi \int_{-1}^1 d\mu' f(\mu' \rightarrow \mu) g(\mu', \lambda) \quad (\text{A1})$$

where λ is the extinction coefficient (least eigenvalue of the characteristic equation), ϖ the particle scattering albedo and $f(\mu' \rightarrow \mu)$ the probability of scattering from μ' to μ , the direction cosines of the incident and scattered photon paths. For isotropic scattering, $f(\mu' \rightarrow \mu) \equiv \frac{1}{2}$ and

$$g(\mu, \lambda) = \frac{\varpi}{2(1 - \lambda\mu)} \quad (\text{A2})$$

and λ satisfies the normalisation [5]

$$1 = \frac{\varpi}{2\lambda} \log\left(\frac{1 + \lambda}{1 - \lambda}\right) \quad (\text{A3})$$

For anisotropic scattering, $g(\mu, \lambda)$ is expanded as a series of Legendre polynomials $P_n(\mu)$ viz.

$$g(\mu, \lambda) = \sum_n (2n + 1) b_n(\lambda) P_n(\mu) \quad (\text{A4})$$

where the coefficients $b_n(\lambda)$ are found from the recursion relation [4]

$$\lambda(n + 1)b_{n+1} - (2n + 1)(1 - \varpi g_n)b_n + \lambda b_{n-1} = 0 \quad (\text{A5})$$

and the g_n are the coefficients of the Legendre expansion of the phase function

$$p(\mu, \mu') = \sum_m (2m + 1) g_m P_m(\mu) P_m(\mu') \quad (\text{A6})$$

e.g. $g_n = g^n$ for Henyey-Greenstein scattering [14] and λ is the extinction coefficient (least eigenvalue of the characteristic equation (eqn (A1))). The eigenvalue λ may be calculated to any desired degree of accuracy from the recursion relation [14]

$$\Delta_n = \frac{(n\lambda)^2}{(2n + 1)(1 - \varpi g_n) - \Delta_{n+1}} \quad (\text{A7})$$

with

$$1 - \varpi = \Delta_1 \quad (\text{A8})$$

Plots of the asymptotic intensity profiles for isotropic and Henyey-Greenstein scattering [15] are presented in Fig. A1.

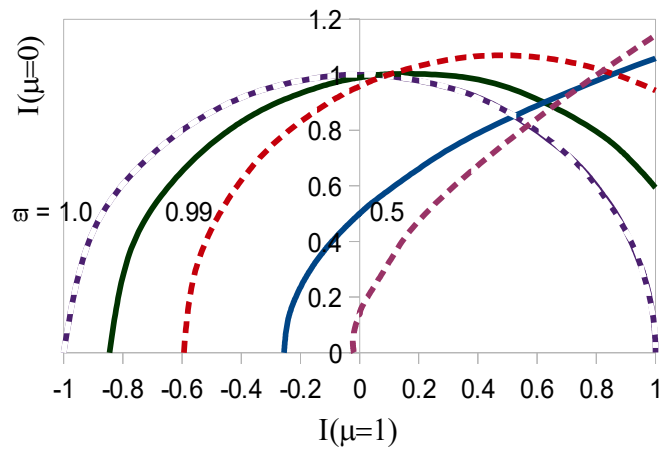
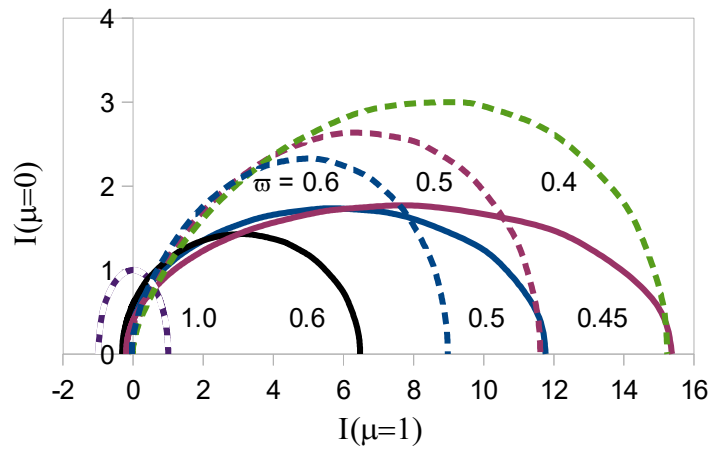


Fig A1

Polar plots of asymptotic radiance for isotropic (cont.) and Henyey-Greenstein (dashed) scattering ($g=0.875$) [15]. Curves labelled with value of scattering albedo ω

Appendix B

The asymptotic fluxes either side of the interface between two refractive half-spaces with constant uniform sources Q_1, Q_2 can be written [5]

$$\begin{aligned} I_1(x < 0, \mu_1) &= Q_1 / 2 - A_1 \exp(\lambda_1 x) g(\lambda_1, -\mu_1) \\ I_1(x > 0, \mu_2) &= Q_2 / 2 - A_2 \exp(-\lambda_2 x) g(\lambda_2, \mu_2) \end{aligned} \quad (\text{B1a,b})$$

and satisfy the boundary equations (cf eqns (15a,b))

$$\begin{aligned} \frac{Q_1}{2} [1 - R_{12}(\mu_1)] - A_1 [g(\lambda_1, \mu_1) - R_{12}(\mu_1) g(\lambda_1, -\mu_1)] \\ = \frac{1}{n^2} [1 - R_{21}(\mu_2^-)] \left[\frac{Q_2}{2} - A_2 g(\lambda_2, -\mu_2^-) \right] \\ \frac{Q_2}{2} [1 - R_{21}(\mu_2)] - A_2 [g(\lambda_2, \mu_2) - R_{21}(\mu_2) g(\lambda_2, -\mu_2)] \\ = n^2 [1 - R_{12}(\mu_1^{\wedge})] \left[\frac{Q_1}{2} - A_1 g(\lambda_1, -\mu_1^{\wedge}) \right] \end{aligned} \quad (\text{B2a,b})$$

the corresponding IBEs for $Q_1 = Q_2 = Q$ are

$$\begin{aligned} C(n_1) A_1 - \frac{F(n_2)}{n^2} A_2 &= \frac{Q}{2} \left(1 - \frac{1}{n^2}\right) T_1 \\ C(n_2) A_2 - n^2 F(n_1) A_1 &= -\frac{Q}{2} (n^2 - 1) T_2 \end{aligned} \quad (\text{B3a,b})$$

with $C(n_i), F(n_i)$ defined by eqns 12(a), 14(b) and T_1, T_2 are the transmission integrals

$$\begin{aligned} T_1 &= \int_0^1 [1 - R_{12}(\mu_1)] \mu_1 d\mu_1 \\ T_2 &= \int_{\mu_c}^1 [1 - R_{21}(\mu_2)] \mu_2 d\mu_2 \end{aligned} \quad (\text{B4a,b})$$

The integrated boundary fluxes are

$$\begin{aligned} \Phi_1(0) &= \frac{Q}{2} + A_1 \int_0^1 g(\lambda_1, -\mu_1) d\mu_1 \\ \Phi_2(0) &= \frac{Q}{2} + A_2 \int_0^1 g(\lambda_2, \mu_2) d\mu_2 \end{aligned} \quad (\text{B5a,b})$$

and the boundary flux discontinuity $\Delta\Phi(0) = \Phi_1(0) - \Phi_2(0)$ for $\lambda_1 = \lambda_2 = \lambda$

$$\Delta\Phi(0) = \frac{A_1 - A_2}{\lambda} \ln \left[\frac{1 + \lambda}{1 - \lambda} \right] = \frac{2(A_1 - A_2)}{\varpi} \quad (\text{B6})$$

The coefficients A_1, A_2 are solutions of the 2x2 matrix equation (B3) with elements $C1, C2, F1, F2, T1, T2$ defined by eqns 12(a), 14(b) and eqn (B4) evaluated by gaussian quadrature and tabulated for $n=1.333333$ in Table B1. The coefficients A_1, A_2 and flux density difference $\Delta\Phi$ for a selection of scattering albedoes are presented in Table B2

2x2 matrix elements

n=1.333333

ω	C1	F2	C2	F1	T2	T1
1	0.466771	0.262559	0.262559	0.466771		
0.9999	0.472848	0.258755	0.270304	0.461299	0.102106	0.102106
0.999	0.486511	0.250902	0.287470	0.449943		
0.99	0.535004	0.229063	0.346169	0.417898		
0.9	0.768772	0.181778	0.604712	0.345838		
0.7	1.336585	0.154454	1.188857	0.302181		
0.4	3.327631	0.143312	3.187069	0.283873		

Table B1

Matrix elements for adjacent half-spaces with uniform internal sources calculated via 128-point gaussian quadrature (N1=N2=64)

ω	M		A	A1		T	T1		$\Delta\Phi$	asyp	K-int
0.4	3.327631	-0.143312	A1	0.029417	T	T1	0.102106				
	-0.283873	3.187069	A2	-0.029417		-T2	-0.102106		0.2942	0.3266	
0.7	1.336585	-0.154454	A1	0.068480	T	T1	0.102106				
	-0.302181	1.188857	A2	-0.068480		-T2	-0.102106		0.3913	0.4058	
0.9	0.768772	-0.181778	A1	0.107418	T	T1	0.102106				
	-0.345838	0.604712	A2	-0.107418		-T2	-0.102106		0.4774	0.4801	
0.99	0.535004	-0.229063	A1	0.133635	T	T1	0.102106				
	-0.417898	0.346169	A2	-0.133635		-T2	-0.102106		0.5399	0.5386	
0.999	0.486511	-0.250902	A1	0.138464	T	T1	0.102106				
	-0.449943	0.287469	A2	-0.138468		-T2	-0.102106		0.5544	0.5533	
0.9999	0.472848	-0.258755	A1	0.139565	T	T1	0.102106				
	-0.461299	0.270304	A2	-0.139565		-T2	-0.102106		0.5583	0.5579	

Table B2

2x2 matrix solutions for adjacent half-spaces with uniform sources
 ω – scattering albedo, **M** – matrix elements, **A** – intensity coefficients,
T – transmission integrals, $\Delta\Phi$ – scalar flux discontinuity, comparing asymptotic and K-integral results [5]

Appendix C

Interface ($x_k = a_k = -a_{k+1}$)

Multilayer diffusion BEs (boundary equations)

$$A_{k+1} \exp(\lambda_{k+1} a_{k+1}) + B_{k+1} \exp(-\lambda_{k+1} a_{k+1}) \quad \varphi_{k+1} = n_{k+1}^2 \varphi_k + C_0(n_{k+1}) J_k \quad (C1a)$$

$$= A_k \exp(-\lambda_k a_k) (n_{k+1}^2 + C_0(n_{k+1}) D_k \lambda_k) + B_k \exp(\lambda_k a_k) (n_{k+1}^2 - C_0(n_{k+1}) D_k \lambda_k) \quad (C1b)$$

$$D_k \lambda_k [A_k \exp(-\lambda_k a_k) - B_k \exp(\lambda_k a_k)] \quad J_k(a_k) = J_{k+1}(-a_{k+1})$$

$$= D_{k+1} \lambda_{k+1} [A_{k+1} \exp(\lambda_{k+1} a_{k+1}) - B_{k+1} \exp(-\lambda_{k+1} a_{k+1})] \quad J(a) = -D \nabla \varphi(a)$$

Multilayer asymptotic IBEs (integrated boundary equations)

$$A_{k+1} \exp(\lambda_{k+1} a_{k+1}) C_{k+1}(n_{k+1}, \lambda_{k+1}) + B_{k+1} \exp(-\lambda_{k+1} a_{k+1}) D_{k+1}(n_{k+1}, \lambda_{k+1}) \quad (C2a)$$

$$= A_k \exp(-\lambda_k a_k) E_k(n_k, \lambda_k) + B_k \exp(\lambda_k a_k) F_k(n_k, \lambda_k)$$

$$A_k \exp(-\lambda_k a_k) D_k(n_k, \lambda_k) + B_k \exp(\lambda_k a_k) C_k(n_k, \lambda_k) \quad (C2b)$$

$$= A_{k+1} \exp(\lambda_{k+1} a_{k+1}) F_{k+1}(n_{k+1}, \lambda_{k+1}) + B_{k+1} \exp(-\lambda_{k+1} a_{k+1}) E_{k+1}(n_{k+1}, \lambda_{k+1})$$

Multilayer diffusion solutions

$$A_{k+1}'' = \frac{1}{2} [n_{k+1}^2 + C_0(n_{k+1}) D_k \lambda_k + \frac{D_k \lambda_k}{D_{k+1} \lambda_{k+1}}] A_k' + \frac{1}{2} [n_{k+1}^2 - C_0(n_{k+1}) D_k \lambda_k - \frac{D_k \lambda_k}{D_{k+1} \lambda_{k+1}}] B_k' \quad (C3a)$$

$$B_{k+1}'' = \frac{1}{2} [n_{k+1}^2 + C_0(n_{k+1}) D_k \lambda_k - \frac{D_k \lambda_k}{D_{k+1} \lambda_{k+1}}] A_k' + \frac{1}{2} [n_{k+1}^2 - C_0(n_{k+1}) D_k \lambda_k + \frac{D_k \lambda_k}{D_{k+1} \lambda_{k+1}}] B_k' \quad (C3b)$$

Multilayer asymptotic solutions

$$A_{k+1}'' = \frac{(D_{k+1} D_k - E_{k+1} E_k) A_k' + (D_{k+1} C_k - E_{k+1} F_k) B_k'}{\det M_{k+1}}$$

$$B_{k+1}'' = -\frac{(F_{k+1} E_k - C_{k+1} D_k) A_k' + (F_{k+1} F_k - C_{k+1} C_k) B_k'}{\det M_{k+1}}$$

$$A_{k+1}'' = A_{k+1} \exp(\lambda_{k+1} a_{k+1}) \quad B_{k+1}'' = B_{k+1} \exp(-\lambda_{k+1} a_{k+1})$$

$$A_k' = A_k \exp(-\lambda_k a_k) \quad B_k' = B_k \exp(\lambda_k a_k)$$

$$\det M_{k+1} = F_{k+1} D_{k+1} - E_{k+1} C_{k+1}, \quad n = n_{k+1} / n_k$$

$$N.B. \det M_{k+1} \equiv 0 \quad (\varpi = 1) \quad (C4)$$

Interface asymptotic coefficients (isotropic scattering)

$$n=1.41(\text{tissue})/1.3348(1\% \text{ saline})=1.0563$$

ϖ	C2	E2	D2	F2	C1	E1	D1	F1
1	0.441182	0.441182	0.441182	0.441182	0.492292	0.492292	0.492292	0.492292
0.995	0.487710	0.484307	0.402083	0.405486	0.537366	0.536970	0.454746	0.455141
0.99	0.509615	0.504805	0.387699	0.392509	0.558698	0.558138	0.441033	0.441593
0.98	0.543705	0.536912	0.368932	0.375725	0.592012	0.591219	0.423238	0.424031
0.97	0.572680	0.564372	0.355669	0.363977	0.620415	0.619442	0.410739	0.411712
0.96	0.599270	0.589691	0.345189	0.354769	0.646542	0.645416	0.400915	0.402040
0.95	0.624532	0.613839	0.336455	0.347148	0.671407	0.670147	0.392763	0.394023
0.9	0.744145	0.729146	0.306211	0.321210	0.789588	0.787791	0.364856	0.366654
0.8	0.997406	0.976624	0.272807	0.293589	1.041168	1.038577	0.334760	0.337351
0.7	1.312770	1.287968	0.253564	0.278367	1.355527	1.352278	0.317874	0.321124
0.6	1.738614	1.710850	0.241340	0.269105	1.780729	1.776853	0.307344	0.311220
0.5	2.352288	2.322314	0.233550	0.263524	2.394004	2.389456	0.300692	0.305240
0.4	3.304258	3.272560	0.228801	0.260499	3.345755	3.340365	0.296605	0.301995
0.3	4.938022	4.904668	0.225897	0.259252	4.979428	4.972755	0.293984	0.300657

Table C1

$$n=1.333333$$

ϖ	C2	E2	D2	F2	C1	E1	D1	F1
1	0.262559	0.262559	0.262559	0.262559	0.466771	0.466771	0.466771	0.466771
1	0.270304	0.266478	0.254929	0.258755	0.472848	0.472388	0.460839	0.461299
0.999	0.28747	0.275367	0.238799	0.250902	0.486511	0.485054	0.448486	0.449943
0.995	0.320125	0.293008	0.210783	0.2379	0.513175	0.509907	0.427682	0.43095
0.99	0.346169	0.307722	0.190617	0.229063	0.535004	0.530364	0.413258	0.417898
0.95	0.476109	0.388421	0.111037	0.198725	0.649513	0.638791	0.361407	0.372128
0.9	0.604712	0.477751	0.054817	0.181778	0.768772	0.752941	0.330006	0.345838
0.8	0.867882	0.680633	-0.023184	0.164065	1.021546	0.996921	0.293104	0.317729
0.7	1.188857	0.951665	-0.082738	0.154454	1.336585	1.302906	0.268503	0.302181
0.6	1.618168	1.337555	-0.131955	0.148659	1.762209	1.71785	0.24834	0.292699
0.5	2.233952	1.915179	-0.173585	0.145187	2.375742	2.317413	0.228649	0.286978
0.4	3.187069	2.832895	-0.210862	0.143312	3.327631	3.248963	0.205205	0.283873
0.3	4.821307	4.426654	-0.252113	0.14254	4.96136	4.848931	0.170164	0.282593

Table C2

Tables of asymptotic coefficients for Fresnel interface calculated via 128-point gaussian quadrature (N1=N2=64)

Half-space albedo vs incidence angle
Diffusion, asymptotic, K-integral, RT data
n=1.333 $\varpi=0.99$

θ deg	α_{diff} diff.	α_{asyp} asyp	$\alpha_{\text{K}2}$ K-int	α_{T} H-int	$\Delta\alpha/\alpha$ diff.%	$\Delta\alpha/\alpha$ asy%	$\Delta\alpha/\alpha$ K-int%
0	0.6667	0.6686	0.6526	0.6519	2.28	2.56	0.11
5	0.6667	0.6686	0.6527	0.6521	2.25	2.53	0.09
10	0.6667	0.6686	0.6533	0.6527	2.15	2.44	0.09
15	0.6668	0.6686	0.6542	0.6536	2.01	2.29	0.09
20	0.6668	0.6687	0.6554	0.655	1.80	2.09	0.06
25	0.6669	0.6688	0.6570	0.6567	1.55	1.84	0.05
30	0.6671	0.669	0.6590	0.6588	1.26	1.55	0.03
35	0.6675	0.6693	0.6615	0.6613	0.93	1.21	0.03
40	0.6682	0.67	0.6644	0.6644	0.56	0.84	0.00
45	0.6693	0.6712	0.6680	0.6681	0.18	0.46	-0.01
50	0.6713	0.6731	0.6725	0.6727	-0.21	0.06	-0.03
55	0.6746	0.6764	0.6783	0.6786	-0.59	-0.32	-0.04
60	0.6801	0.6819	0.6863	0.6866	-0.94	-0.68	-0.04
65	0.6895	0.6912	0.6977	0.6981	-1.24	-0.99	-0.06
70	0.7052	0.7069	0.7150	0.7154	-1.42	-1.19	-0.06
75	0.7321	0.7336	0.7424	0.7428	-1.44	-1.24	-0.05
80	0.7782	0.7794	0.7877	0.788	-1.24	-1.09	-0.04
85	0.8583	0.8591	0.8648	0.865	-0.77	-0.68	-0.02
90	1.0000	1.0000	1.0000	1.0000	0.00	0.00	0.00

Table I

Half-space albedo α vs angle of incidence. Plane-wave surface source (n=1.333 $\varpi=0.99$). Comparison of diffusion, asymptotic and K-integral values vs radiative transfer (H-int) [8]

planar

ϖ	α_{diff} diffusion	α_s	α_{asy} asymp.	α_{K2} K-int.	α_T H-int.
0.995	0.7476	0.8114	0.7484	0.7357	0.7352
0.99	0.6667	0.6657	0.6686	0.6526	0.6519
0.98	0.5691	0.5667	0.5734	0.5543	
0.97	0.5049	0.5009	0.5116	0.4911	
0.96	0.4566	0.4510	0.4657	0.4447	
0.95	0.4178	0.4106	0.4293	0.4081	0.4070
0.9	0.2926	0.2773	0.3149	0.2952	0.2940
0.8	0.1656	0.1346	0.2056	0.1910	
0.7	0.0936	0.0473	0.1477	0.1375	0.1364
0.6	0.0444	-0.0168	0.1104	0.1036	
0.5	0.0077	-0.0682	0.0841	0.0796	0.0792
0.4	-0.0213	-0.1115	0.0645	0.0615	
0.3	-0.0450	-0.1488	0.0494	0.0472	0.0480
0.2	-0.0649	-0.1806	0.0389	0.0351	
0.1	-0.0820	-0.2071			
0	-0.0969	-0.2292	0.0204	0.0204	0.0204

isotropic

ϖ	α_{diff} diffusion	α_s	α_{asy} asymp.	α_{K2} K-int.	α_T H-int.
0.995	0.7304	0.7912	0.7602	0.7584	0.7584
0.99	0.6533	0.6523	0.6842	0.6812	0.6813
0.98	0.5603	0.5580	0.5935	0.5891	
0.97	0.4991	0.4953	0.5346	0.5293	
0.96	0.4530	0.4477	0.4908	0.4851	
0.95	0.4161	0.4092	0.4561	0.4501	0.4501
0.9	0.2967	0.2822	0.3471	0.3408	0.3409
0.8	0.1758	0.1462	0.2430	0.2383	
0.7	0.1072	0.0630	0.1876	0.1849	0.1850
0.6	0.0603	0.0019	0.1522	0.1509	
0.5	0.0253	-0.0471	0.1271	0.1270	0.1271
0.4	-0.0023	-0.0884	0.1084	0.1091	
0.3	-0.0249	-0.1239	0.0942	0.0953	0.0950
0.2	-0.0440	-0.1542	0.0868	0.0879	
0.1	-0.0603	-0.1795			
0	-0.0745	-0.2005	0.0187	0.0187	0.0187

Tables II a, b

Half-space albedo α vs scattering albedo ϖ , normally incident plane-wave and isotropic sources ($n=1.333$) [8, 13]. The column headed α_s is calculated using accurate values of the diffusion coefficient D (eq (27))

ω	A*	T*	A*	T*	A*	T*	A*	T*
	diffusion		asymptotic		K-integral		RT	
1	0.79781	0.20219	0.79781	0.20219	0.79447	0.20553	0.79445	0.20555
0.9999	0.79523	0.20030	0.79524	0.20029	0.79190	0.20363		
0.9995	0.78518	0.19299			0.78188	0.19629		
0.999	0.77317	0.18442	0.77333	0.18431	0.76994	0.18766		
0.995	0.69497	0.13234			0.69244	0.13507		
0.99	0.62603	0.09260	0.62924	0.09221	0.62461	0.09487		
0.98	0.53507	0.05116	0.54221	0.05097	0.53641	0.05283		
0.97	0.47452	0.03127	0.48555	0.03123	0.47902	0.03256		
0.96	0.42948	0.02040	0.44426	0.02045	0.43730	0.02144		
0.95	0.39375	0.01394	0.41212	0.01405	0.40493	0.01479		
0.9	0.28059	0.00316	0.31507	0.00330	0.30803	0.00355		
0.8	0.16728	0.00045	0.22780	0.00052	0.22268	0.00057		
0.7	0.10162	0.00012	0.18378	0.00016	0.18036	0.00018	0.18034	0.00018
0.6	0.05504	0.00005	0.15616	0.00008	0.15413	0.00008		
0.5	0.01863	0.00003	0.13699	0.00005	0.13603	0.00004		
0.4	-0.01140	0.00002	0.12289	0.00004	0.12271	0.00002		
0.3	-0.03678	0.00002	0.11215	0.00004	0.11247	0.00001	0.11245	0.00002

Table III

Albedo A^* and diffuse transmittance T^* of dielectric slabs for isotropic surface illumination, isotropic scattering ($n=1.5$, $d=10$). Note near 5-figure agreement of K-integral values with RT data (bold italic) [12, 13]

ϖ	diffusion $\Delta\Phi$	asympt. $\Delta\Phi$	K-int* $\Delta\Phi$	diff. $\delta\%$	asy. $\delta\%$
1.0000	0.5600	0.5600	0.5600	0.00	0.00
0.9999	0.5583	0.5583	0.5579	-0.07	-0.07
0.999	0.5548	0.5544	0.5533	-0.27	-0.20
0.99	0.5438	0.5399	0.5386	-1.0	-0.2
0.98	0.5373	0.5298	0.5285	-1.7	-0.2
0.97	0.5323	0.5213	0.5203	-2.3	-0.2
0.96	0.5281	0.5138	0.5131	-2.9	-0.1
0.95	0.5245	0.5068	0.5067	-3.5	0.0
0.9	0.5101	0.4774	0.4801	-6.2	0.6
0.85	0.4989	0.4527			
0.8	0.4892	0.4306	0.4394	-11.3	2.0
0.75	0.4804	0.4103			
0.7	0.4721	0.3913	0.4058	-16.3	3.6
0.65	0.4642	0.3734			
0.6	0.4565	0.3562	0.3758	-21.5	5.2
0.55	0.4490	0.3398			
0.5	0.4415	0.3249	0.3490	-26.5	6.9
0.45	0.4340	0.3088			
0.4	0.4265	0.2942	0.3266	-30.6	9.9

*mmrw [5]

Table IV

Interface flux density discontinuity $\Delta\Phi$ vs ϖ (uniform sources, $n_2/n_1=4/3$)

Comparison of diffusion, asymptotic, K-integral results and relative error $\delta\%$

ω	diffusion		asymptotic		K-integral		RT	
	A*	T*	A*	T*	A*	T*	A*	T*
1	0.77688	0.17541	0.81247	0.18753	0.80927	0.19073	0.80926	0.19075
0.999	0.75630	0.16177	0.79252	0.17188				
0.99	0.62549	0.08694	0.66844	0.0888	0.66457	0.09148		
0.95	0.39048	0.01467	0.45473	0.01418				
0.9	0.26348	0.00352	0.3468	0.00339	0.34061	0.00366		
0.8	0.12751	0.00053	0.2429	0.00054				
0.7	0.04434	0.00015	0.18773	0.00017	0.18489	0.00019	0.18499	0.00019
0.6	-0.01675	0.00007	0.15222	0.00008				
0.5	-0.06054		0.12713	0.00005	0.12695	0.00004		
0.4	-0.10706		0.10844	0.00004				
0.3			0.09402	0.00004	0.09515	0.00001	0.095	0.00002

Table V

Double-layer albedo A^* , diffuse transmittance T^* vs scattering albedo ω
 $(n_1 = 1.333 \ n_2 = 1.5 \ 2a = 10)$ isotropic source, isotropic scattering [12]

$n_1=1.333$ $n_2=1.5$ $2a=10$

ϖ_1	ϖ_2	A*	T*	A*	T*	A*	T*
		asymptotic		K-integral		RT	
1	0.7	0.69223	0.00387	0.68974	0.00374	0.68976	0.00374
1	0.3	0.68196	0.00192	0.67968	0.00036	0.67967	0.00108
1	1	0.81251	0.18749	0.80927	0.19073	0.80926	0.19075
0.7	1	0.18789	0.00403	0.18501	0.00437	0.18511	0.00441
0.3	1	0.09405	0.00142	0.09515	0.00034	0.09501	0.00109

$n_1=1.5$ $n_2=1.333$ $2a=10$

1	1	0.80984	0.19016			0.80926	0.19075
0.7	0.7	0.18379	0.00018			0.18035	0.00019
0.3	0.3	0.11215	0.00004			0.11245	0.00002
0.7	1	0.1839	0.00325	0.1805	0.00414	0.18046	0.00374
1	0.7	0.65529	0.00509	0.65655	0.00517	0.65897	0.00441
0.3	1	0.11218	0.00121			0.11246	0.00108
1	0.3	0.63808	0.00234			0.64144	0.00109

$n_1=1.5$ $n_2=1.5$ $2a=10$

1	1	0.79781	0.20219	0.79447	0.20553	0.79445	0.20555
---	---	---------	---------	---------	---------	---------	---------

$n_1=1.5$ $n_2=3$ $2a=10$

0.3	0.3	0.11216	0.11247	0.11245	0.00002	0.00001	0.00002
0.3	0.7	0.11216		0.11245	0.00002		0.00003
0.3	1	0.11218	0.11247	0.11246	0.00145	0.00038	0.0012
0.7	0.3	0.18377		0.18033	0.00005		0.00005
0.7	0.7	0.18377		0.18034	0.00005		0.00009
0.7	1	0.18389	0.18046	0.18045	0.00416	0.00468	0.0047
1	0.3	0.64019	0.63634	0.63632	0.00121	0.00054	0.00094
1	0.7	0.64329	0.6409	0.63924	0.00123	0.00164	0.00178
1	1	0.77335	0.77029	0.77008	0.22665	0.22971	0.22991

$n_1=1$ $n_2=1$ $2a=10$

0.995	0.8	0.77666	0.00655	0.77938	0.00608	0.77939	0.00609
-------	-----	---------	---------	---------	---------	---------	---------

Table VI

Double-layer albedo A*, diffuse transmittance T* vs scattering albedo ϖ , isotropic source, isotropic scattering [12]

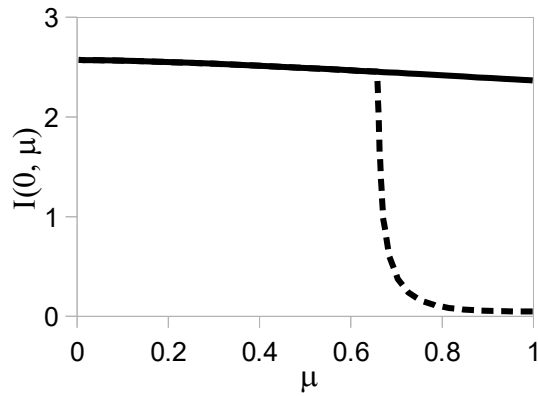


Fig. 1

Refractive 'hole' in reflected angular intensity at inner surface boundary (incident profile: continuous, reflected: dashed). Half-space ($n = 1.333$), plane-wave source, normal incidence, isotropic scattering, $\varpi=0.99$)

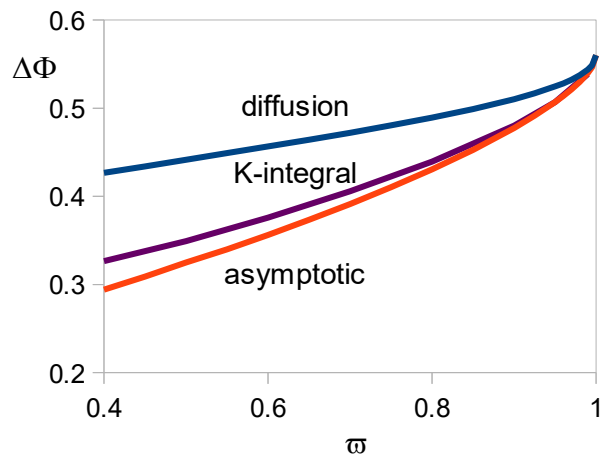
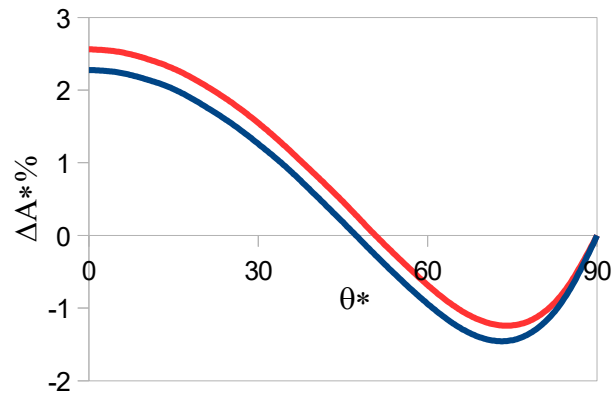
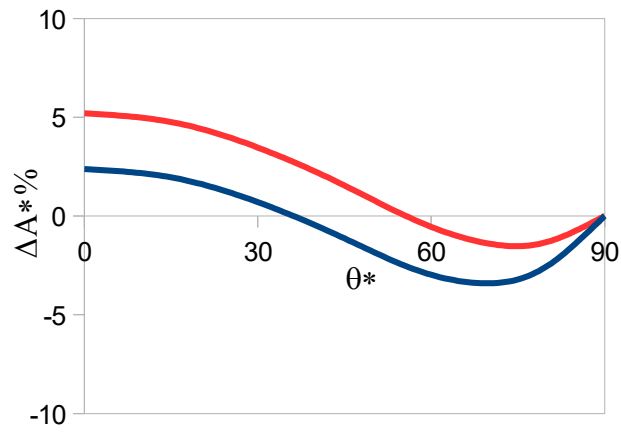


Fig 2

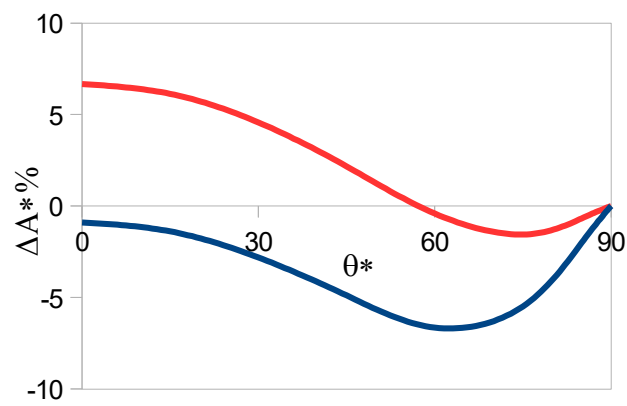
Comparison of diffusion, asymptotic transport and K-integral results for flux density discontinuity at an interface between two scattering media of differing refractive index vs scattering albedo ϖ (refractive index ratio $n = 4/3$, isotropic scattering) [5, 13]



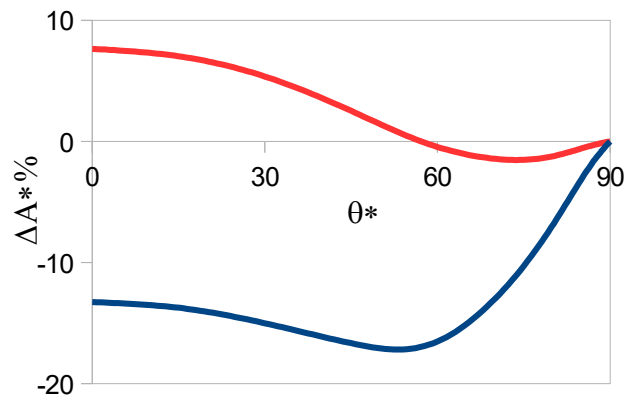
(a) $\omega = 0.99$



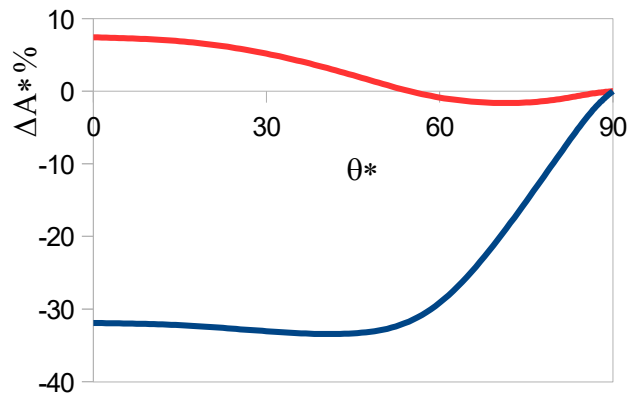
(b) $\omega = 0.95$



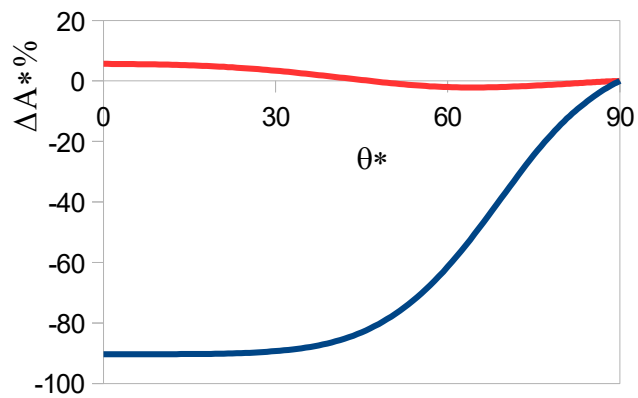
(c) $\omega = 0.9$



(d) $\omega=0.8$

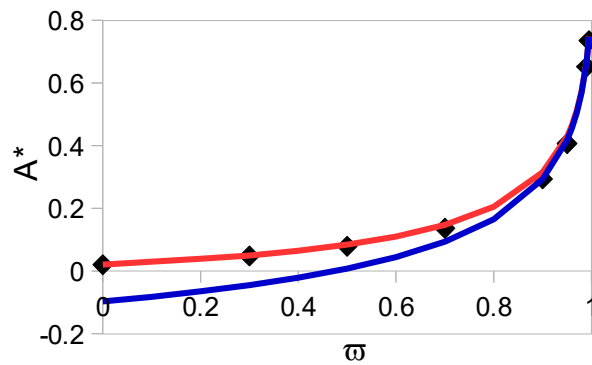


(e) $\omega=0.7$

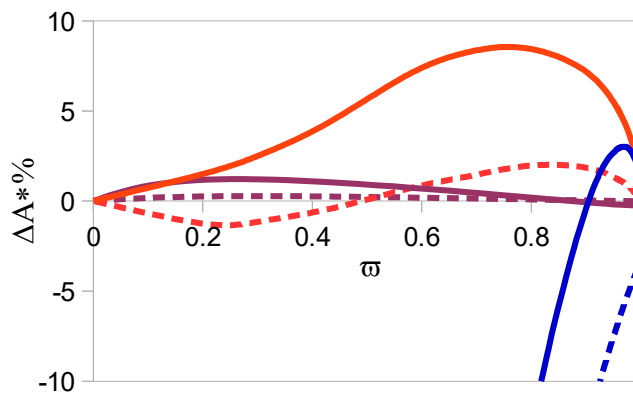


(f) $\omega=0.5$

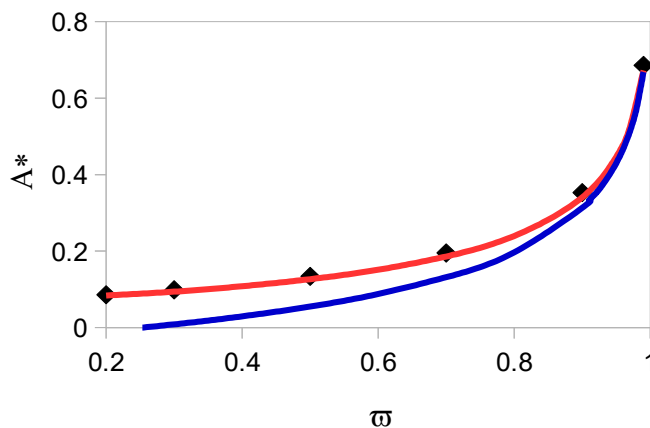
Half-space albedo error $\Delta A^*%$ vs plane wave angle of incidence θ^* for a range of scattering albedo $0.99 \geq \omega \geq 0.5$ (asymptotic - red, diffusion - blue, $n=1.333$)
 Figs 3(a-f).



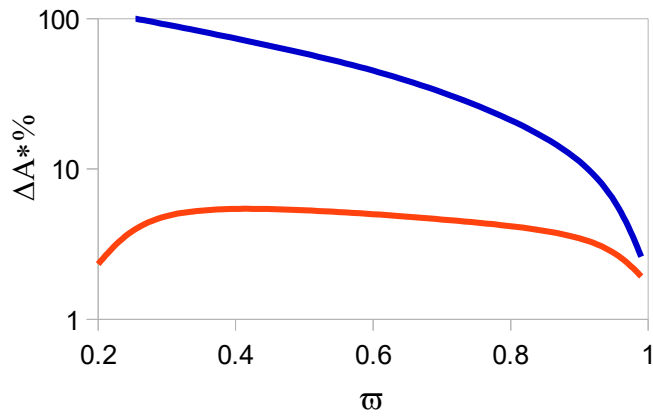
a) Half-space albedo A^* vs scattering albedo ω . Plane-wave source, normal incidence, Fresnel boundary ($n=1.333$). Diffusion (blue), asymptotic (red), RT (\blacklozenge)



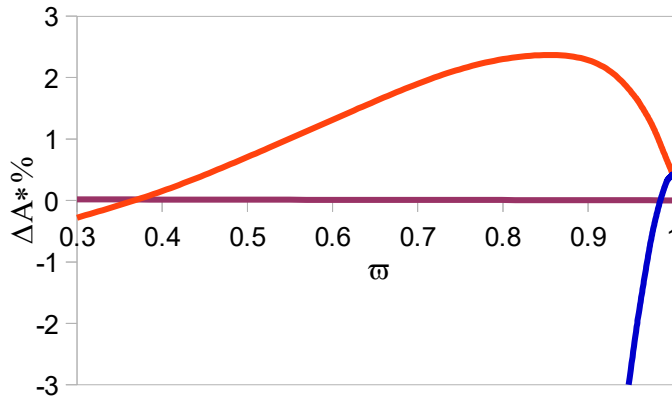
b) Half-space albedo error $\Delta A^* \%$ vs ω : planar (cont.) and isotropic (dashed) sources. Diffusion (blue), asymptotic (red), K-integral (bordeaux) ($n=1.333$)



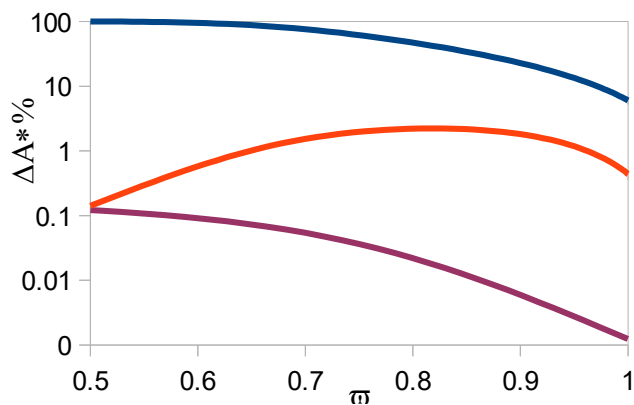
c) Half-space albedo A^* vs scattering albedo ω . Plane-wave source (normal incidence), diffusing surface boundary ($n=1.333$). Asymptotic (red), diffusion (blue), RT (\blacklozenge)



d) Half-space albedo error ΔA^* % vs scattering albedo ω . Asymptotic (red), diffusion (blue), diffusing boundary. Parameters as above



e) Slab albedo error ΔA^* % vs scattering albedo ω ($n=1.5$ $d=10$)
Diffusion (blue), asymptotic (red), K-integral (bordeaux), isotropic source



f) Double-layer albedo error $|\Delta A^*|$ % vs ω : diffusion (blue), asymptotic (red), K-integral (bordeaux). Isotropic source ($n_1 = 1.333$, $n_2 = 1.5$, $2a = 10$)

Figs 4(a-f)

Supplement: Boundary fluxes

Further analysis of the angular intensity profiles corresponding to the diffusion, asymptotic and K-integral approximations reveals increasingly large errors in the internal intensity incident at the boundary $I(0, -\mu)$ for $\mu \leq \mu_c$ i.e. the region of total internal reflection, reaching a maximum error at $\mu=0$ (grazing incidence: $\theta=90$ deg). While having a small effect on external quantities, such as albedo A^* and diffuse transmittance T^* (comprising the transmitted light), this introduces significant errors in the internal scalar flux ϕ (fluence) at the boundary, even for the K-integral analysis. The boundary error is significantly lower for an isotropic source compared with plane-wave illumination.

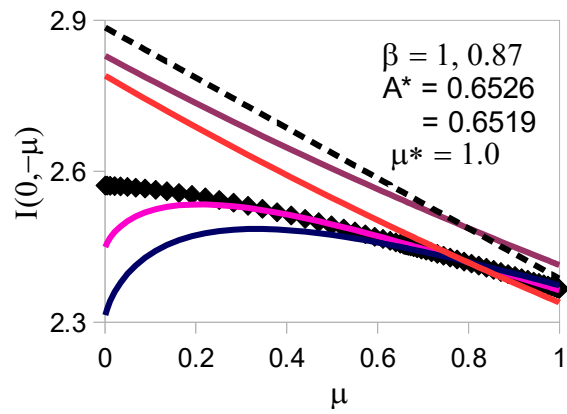
The boundary transient $\psi(0, \mu)$ used for the K-integral analysis takes the modified form

$$\psi(0, -\mu) \approx 1 - \beta \mu \ln \left(1 + \frac{1}{\mu} \right) \quad (\text{S1})$$

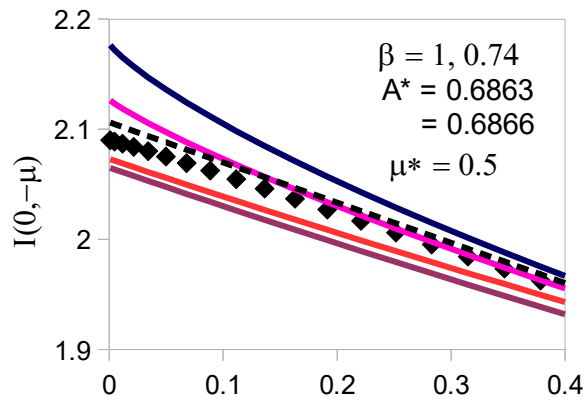
where $\beta \sim 1$ is a fitting parameter chosen to match the albedo A^* given by RT theory [13]. However, the scalar flux error at the boundary, though reduced in this case, remains finite, requiring further development of the boundary transient to correct the error [5].

Results for half-space boundary fluxes are presented in the following for plane-wave and isotropic sources, comparing diffusion, asymptotic and K-integral predictions[‡] for $I(0, \mu)$, $J(0, \mu)$, $\phi(0, \mu)$ and $\phi(0)$ with accurate radiative transfer (RT) values [8]

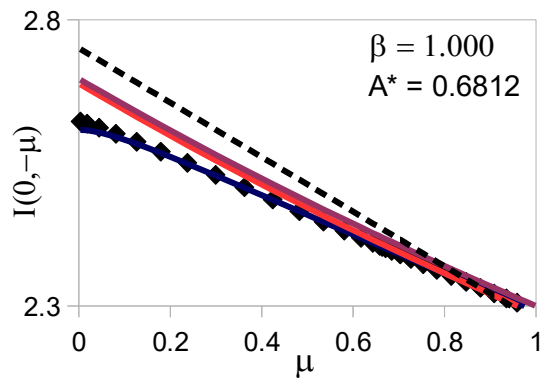
[‡]The K-integrals are evaluated for $\psi(0, -\mu)$ constant (K1), log transient (as above) with $\beta=1$ (K2) and for $\beta=\beta'$ (K2') adjusted to fit the accurate RT albedo A^* . The integrals are calculated using gaussian quadrature, dividing the range of integration into two intervals either side of the cosine of the critical angle μ_c viz. $\mu \in |0, \mu_c|$ and $\mu \in |\mu_c, 1|$.



(a)



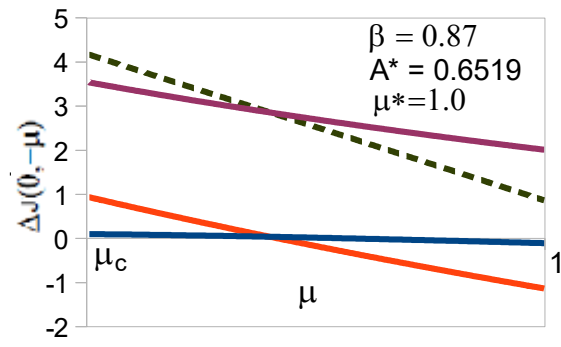
..
(b)



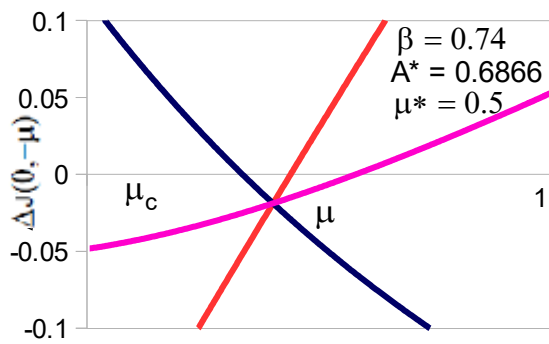
(c)

Internal intensity $I(0,-\mu)$ incident at the boundary of a half-space vs μ ($n = 1.333$, $\varpi = 0.99$). Diffusion (dashed), asymptotic (bordeaux), K-integral (K1: red, K2: blue, K2': pink), RT (\blacklozenge). Plane-wave surface source incident at $\mu^* = 1$ (a), 0.5 (b); isotropic source (c)

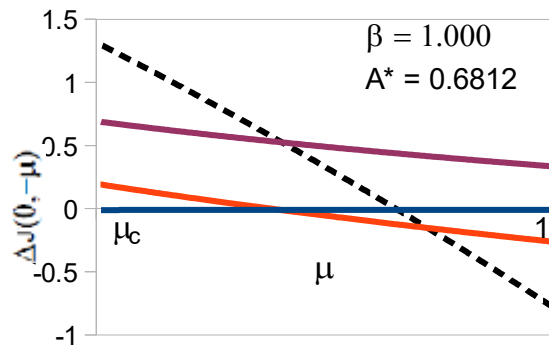
Fig S1



(a)



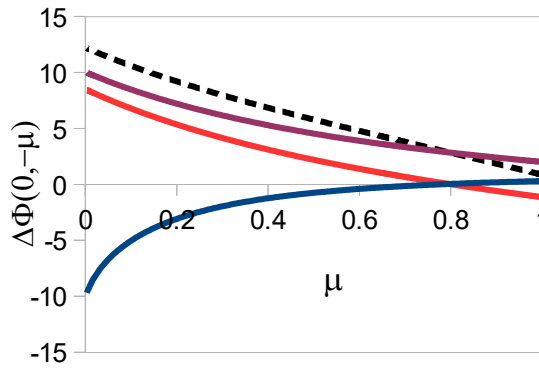
(b)



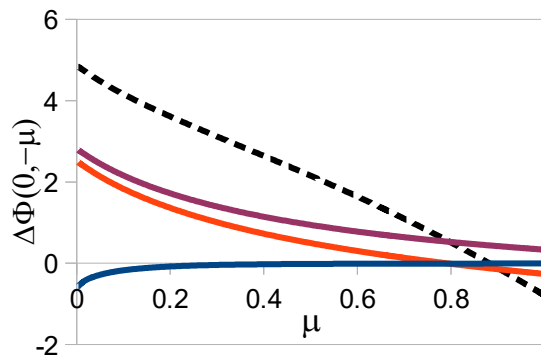
(c)

Percentage error $\Delta J(0, -\mu)$ at the boundary of a half-space vs μ ($n = 1.333$, $\varpi = 0.99$). Diffusion (dashed), asymptotic (bordeaux), K-integral (K1: red, K2: blue, K2': pink). Plane-wave surface source incident at $\mu^* = 1$ (a), 0.5 (b); isotropic source (c)

Fig S2

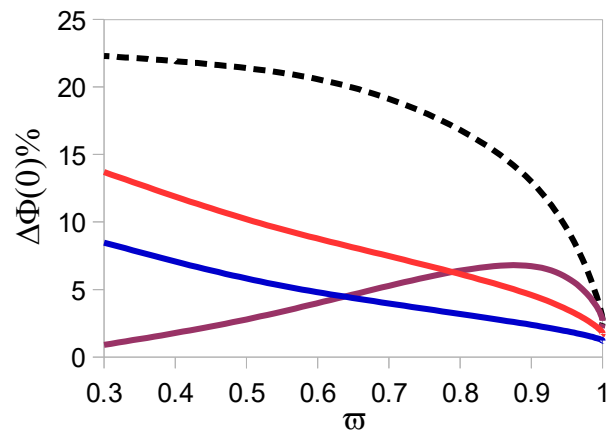


Percentage error $\Delta\Phi(0,-\mu)$ at the boundary of a half-space vs μ ($n = 1.333$, $\varpi = 0.99$). Diffusion (dashed), asymptotic (bordeaux), K-integral (K1: red, K2: blue). Plane-wave source at normal incidence

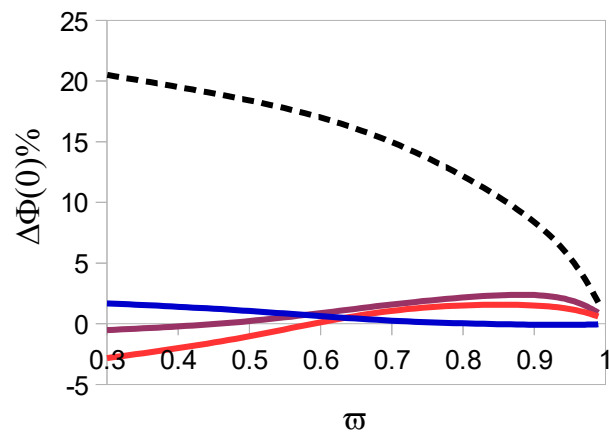


Percentage error $\Delta\Phi(0,-\mu)$ at the boundary of a half-space vs μ ($n = 1.333$, $\varpi = 0.99$). Diffusion (dashed), asymptotic (bordeaux), K-integral (K1: red, K2: blue). Isotropic surface source

Fig S3



Half-space boundary flux error $\Delta\Phi(0)\%$ vs ω ($n=1.333333$)
 Planar source: diffusion (dashed), asymptotic (bordeaux),
 K-integrals (K1: red, K2: blue)



Half-space boundary flux error $\Delta\Phi(0)\%$ vs ω ($n=1.333333$)
 Lambertian source: diffusion (dashed), asymptotic (bordeaux),
 K-integrals (K1: red, K2: blue)

Fig S4

Half-space boundary fluxes: planar source, normal incidence, isotropic scattering $n=4/3$

algorithm	$\Phi(0)$	$\Delta\Phi(0)$	$J(0)$	$\alpha(n, \nu)$	
H-integral	7.200788	%	0.84815	0.868558	β', β
K-integral2	7.178994	-0.302654	0.84815	0.868558	0.854
K-integral2	7.116257	-1.173914	0.848387	0.868795	1
K-integral1	7.316965	1.613395	0.84763	0.868038	
asypm	7.356179	2.157974	0.854984	0.875392	
diffusion	7.363664	2.261929	0.854911	0.875319	

$\varpi=0.999$

algorithm	$\Phi(0)$	$\Delta\Phi(0)$	$J(0)$	$\alpha(n, \nu)$	
H-integral	5.957014	%	0.631509	0.651917	β', β
K-integral2	5.935487	-0.361373	0.63151	0.651918	0.87
K-integral2	5.872399	-1.420434	0.632158	0.652566	1
K-integral1	6.094155	2.302171	0.62988	0.650288	
asypm	6.188169	3.880381	0.648208	0.668616	
diffusion	6.241073	4.768472	0.646345	0.666753	

$\varpi=0.99$

algorithm	$\Phi(0)$	$\Delta\Phi(0)$	$J(0)$	$\alpha(n, \nu)$	
H-integral	3.740997	%	0.273533	0.293942	β', β
K-integral2	3.716931	-0.643321	0.273536	0.293944	0.89
K-integral2	3.651789	-2.384616	0.274779	0.295187	1.00
K-integral1	3.912626	4.587766	0.2698	0.290208	
asypm	3.99264	6.726612	0.29447	0.314879	
diffusion	4.226983	12.99082	0.272147	0.292555	

$\varpi=0.9$

algorithm	$\Phi(0)$	$\Delta\Phi(0)$	$J(0)$	$\alpha(n, \nu)$	
H-integral	2.649565	%	0.115961	0.136369	β', β
K-integral2	2.628043	-0.812276	0.115954	0.136362	0.88
K-integral2	2.544671	-3.958924	0.117067	0.137475	1.00
K-integral1	2.847377	7.465806	0.113025	0.133433	
asypm	2.789232	5.271308	0.127268	0.147676	
diffusion	3.156256	19.12354	0.073216	0.093625	

$\varpi=0.7$

algorithm	$\Phi(0)$	$\Delta\Phi(0)$	$J(0)$	$\alpha(n, \nu)$	
H-integral	2.218628	%	0.058771	0.079179	β', β
K-integral2	2.314958	4.341849	0.05877	0.079179	0.626
K-integral2	2.089781	-5.807536	0.059195	0.079604	1
K-integral1	2.444514	10.18133	0.058526	0.078934	
asypm	2.280315	2.780388	0.063666	0.084074	
diffusion	2.69383	21.41869	-0.012698	0.00771	

$\varpi=0.5$

Half-space boundary fluxes: Lambertian source, isotropic scattering (n=4/3)

algorithm	$\Phi(0)$	$\Delta\Phi(0)$	$J(0)$	$\alpha(n, \nu)$	
H-integral	5.844054	%	0.614815	0.681274	β', β
K-integral2	5.833747	-0.176358	0.614816	0.681274	1.067
K-integral2	5.841385	-0.045666	0.614737	0.681196	1
K-integral1	5.879458	0.605817	0.614346	0.680805	
asypm	5.897265	0.910523	0.617736	0.684194	
diffusion	5.947689	1.773346	0.615961	0.68242	

$\varpi=0.99$

algorithm	$\Phi(0)$	$J(0)$	$\alpha(n, \nu)$	$\Delta\Phi(0)$
H-integral	4.43004	0.383638	0.450097	%
K-integral2	4.426343	0.383609	0.450067	-0.083446
K-integral1	4.483636	0.382621	0.44908	1.209847
asypm	4.517684	0.38968	0.456139	1.978417
diffusion	4.670594	0.37874	0.445198	5.430068

$\varpi=0.95$

algorithm	$\Phi(0)$	$J(0)$	$\alpha(n, \nu)$	$\Delta\Phi(0)$
H-integral	3.716808	0.27442	0.340879	%
K-integral2	3.714031	0.27439	0.340848	-0.074708
K-integral1	3.772936	0.273265	0.339724	1.510109
asypm	3.80484	0.280647	0.347106	2.368477
diffusion	4.028234	0.259383	0.325841	8.378861

$\varpi=0.9$

algorithm	$\Phi(0)$	$J(0)$	$\alpha(n, \nu)$	$\Delta\Phi(0)$
H-integral	2.616493	0.118538	0.184997	%
K-integral2	2.623319	0.118434	0.184893	0.260871
K-integral1	2.644444	0.118152	0.184611	1.068258
asypm	2.658079	0.121296	0.187754	1.589369
diffusion	3.007865	0.069787	0.136246	14.95787

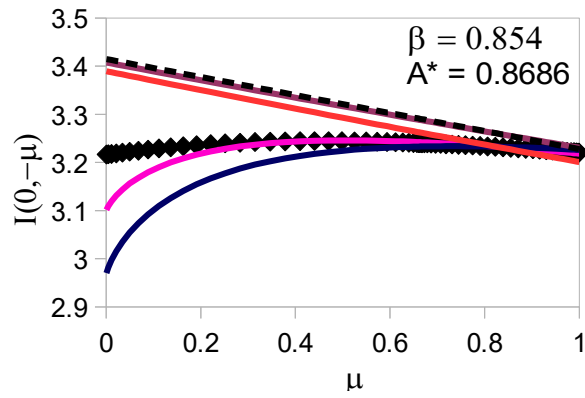
$\varpi=0.7$

algorithm	$\Phi(0)$	$J(0)$	$\alpha(n, \nu)$	$\Delta\Phi(0)$
H-integral	2.168218	0.060591	0.12705	%
K-integral2	2.191145	0.060507	0.126965	1.057417
K-integral1	2.145857	0.060592	0.127051	-1.031318
asypm	2.173105	0.060679	0.127137	0.225382
diffusion	2.567187	-0.012095	0.054363	18.40076

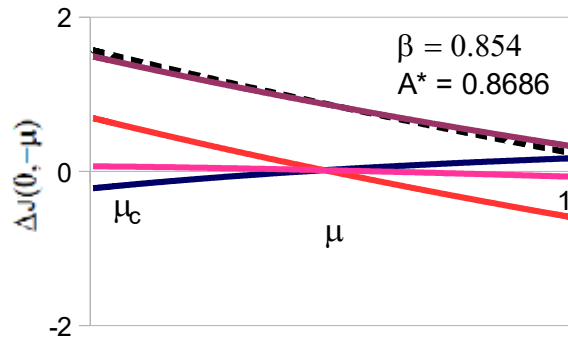
$\varpi=0.5$

algorithm	$\Phi(0)$	$J(0)$	$\alpha(n, \nu)$	$\Delta\Phi(0)$
H-integral	1.905995	0.028582	0.095041	%
K-integral2	1.938157	0.028823	0.095282	1.687414
K-integral1	1.852	0.027911	0.094369	-2.832862
asypm	1.896006	0.027706	0.094165	-0.524044
diffusion	2.296827	-0.062331	0.004127	20.50541

$\varpi=0.3$



(a)



(b)

Fig S5

Half-space boundary values (plane-wave, normal incidence: $n=1.333$, $\varpi=0.999$, gaussian quadrature: $N1=N2=32$). Diffusion (dashed), asymptotic (bordeaux), K-integral (K1: red, K2: blue, K2': pink). (a) internal intensity $I(0, -\mu)$ vs μ
 (b) % error $\Delta J(0, -\mu)$ in boundary current $J(\mu)$ vs μ for $\mu \in |\mu_c, 1|$

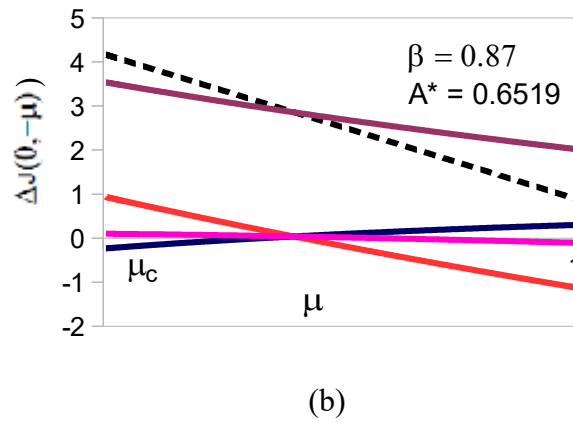
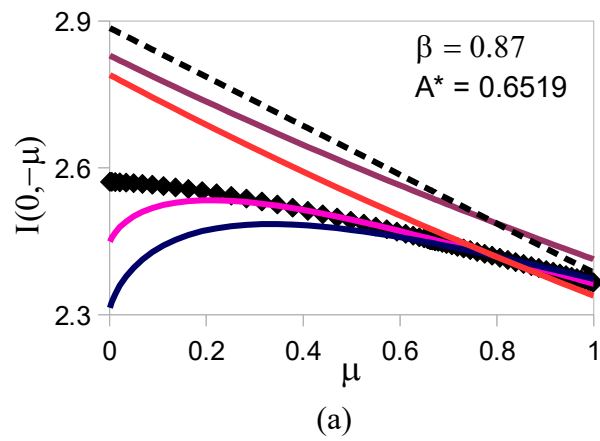
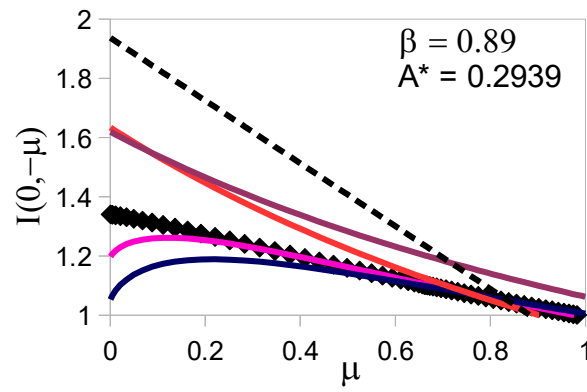
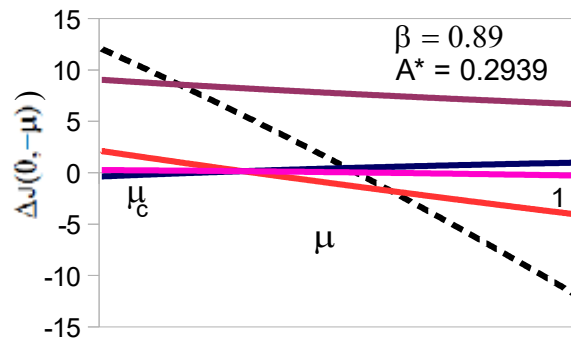


Fig S6

Half-space boundary values (plane-wave, normal incidence: $n=1.333$, $\varpi=0.99$, gaussian quadrature $N1=N2=32$). Diffusion (dashed), asymptotic (bordeaux), K-integral (K1: red, K2: blue, K2': pink). (a) internal intensity $I(0, -\mu)$ vs μ (b) % error $\Delta J(0, -\mu)$ in boundary current $J(\mu)$ vs μ for $\mu \in |\mu_c, 1|$



(a)



(b)

Fig S7

Half-space boundary values (plane-wave, normal incidence: $n=1.333$, $\varpi=0.9$, gaussian quadrature $N1=N2=32$). Diffusion (dashed), asymptotic (bordeaux), K-integral (K1: red, K2: blue, K2': pink). (a) internal intensity $I(0, -\mu)$ vs μ (b) % error $\Delta J(0, -\mu)$ in boundary current $J(\mu)$ vs μ for $\mu \in |\mu_c, 1|$

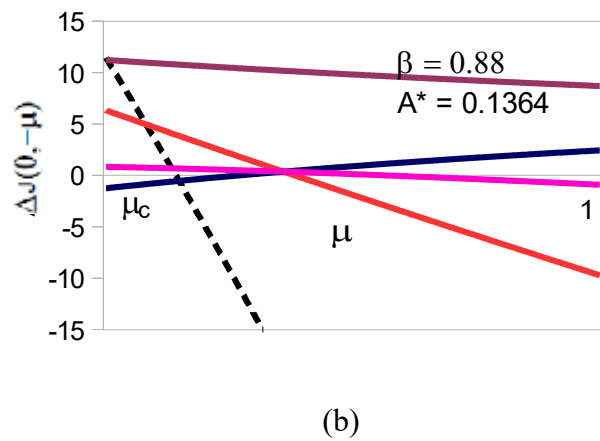
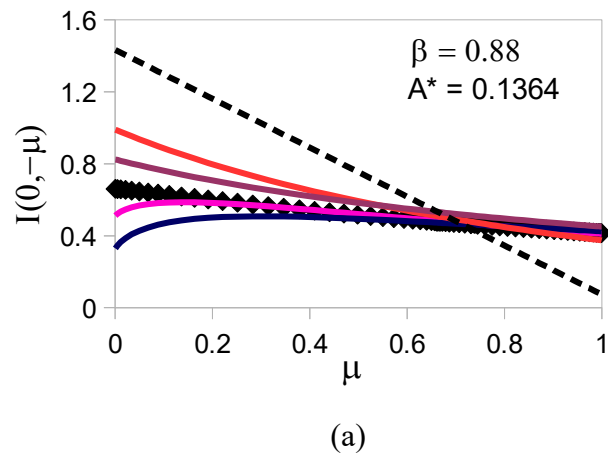
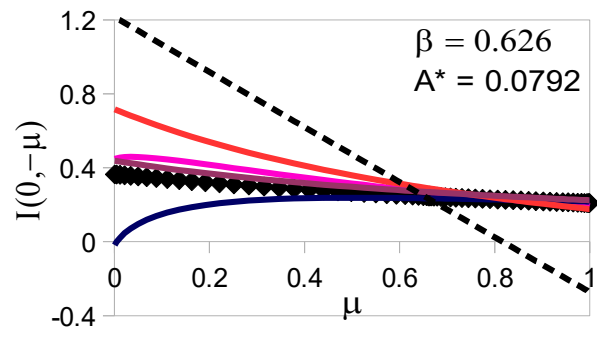
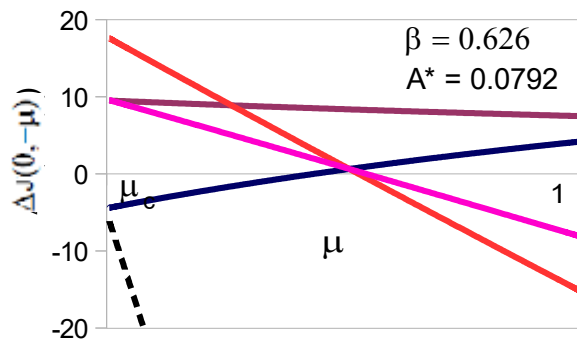


Fig S8

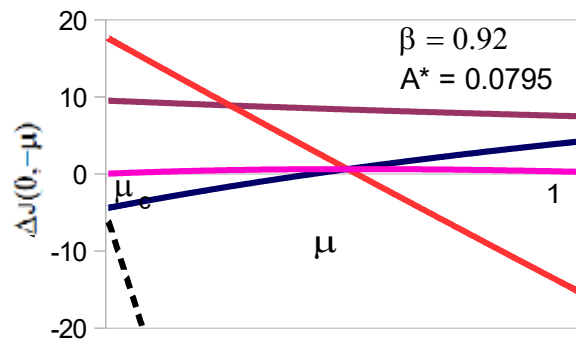
Half-space boundary values (plane-wave, normal incidence: $n=1.333$, $\varpi=0.7$, gaussian quadrature $N1=N2=32$). Diffusion (dashed), asymptotic (bordeaux), K-integral (K1: red, K2: blue, K2': pink). (a) internal intensity $I(0, -\mu)$ vs μ (b) % error $\Delta J(0, -\mu)$ in boundary current $J(\mu)$ vs μ for $\mu \in |\mu_c, 1|$



(a)



(b)



(c)

Fig S9

Half-space boundary values (plane-wave, normal incidence: $n=1.333$, $\varpi=0.5$, gaussian quadrature $N1=N2=32$). Diffusion (dashed), asymptotic (bordeaux), K-integral (K1: red, K2: blue, K2': pink). (a) internal intensity $I(0, -\mu)$ vs μ (b, c) % error $\Delta J(0, -\mu)$ in boundary current $J(\mu)$ vs μ for $\mu \in |\mu_c, 1|$